Effect of cation on diffusion coefficient of ionic liquids at onion-like carbon electrodes

2014 J. Phys.: Condens. Matter 26 284104

(http://iopscience.iop.org/0953-8984/26/28/284104)

IOP Publishing Journal of Physics: Condensed Matter
J. Phys.: Condens. Matter **26** (2014) 284104 (10pp) doi:10.1088/0953-8984/26/28/284104

Effect of cation on diffusion coefficient of ionic liquids at onion-like carbon electrodes

Katherine L Van Aken[1], John K McDonough[1], Song Li[2], Guang Feng[2], Suresh M Chathoth[3,5], Eugene Mamontov[3], Pasquale F Fulvio[4], Peter T Cummings[2], Sheng Dai[4] and Yury Gogotsi[1]

[1] Department of Materials Science and Engineering & A J Drexel Nanomaterialstechnology Institute, Drexel University, Philadelphia, PA 19104, USA
[2] Department of Chemical and Biomolecular Engineering, Vanderbilt University, Nashville, TN 37235, USA
[3] Chemical and Engineering Materials Division, Neutron Sciences Directorate, Oak Ridge National Laboratory, Oak Ridge, TN 37831, USA
[4] Chemical Science Division, Oak Ridge National Laboratory, Oak Ridge, TN 37831, USA
[5] Department of Physics and Materials Science, City University of Hong Kong, Hong Kong, China

E-mail: gogotsi@drexel.edu

Received 26 October 2013, revised 14 January 2014
Accepted for publication 23 January 2014
Published 12 June 2014

Abstract

While most supercapacitors are limited in their performance by the stability of the electrolyte, using neat ionic liquids (ILs) as the electrolyte can expand the voltage window and temperature range of operation. In this study, ILs with bis(trifluoromethylsulfonyl) imide (Tf2N) as the anion were investigated as the electrolyte in onion-like carbon-based electrochemical capacitors. To probe the influence of cations on the electrochemical performance of supercapacitors, three different cations were used: 1-ethyl-3-methylimidazolium, 1-hexyl-3-methylimidazolium and 1,6-bis(3-methylimidazolium-1-yl). A series of electrochemical characterization tests was performed using cyclic voltammetry (CV), galvanostatic cycling and electrochemical impedance spectroscopy (EIS). Diffusion coefficients were measured using EIS and correlated with quasielastic neutron scattering and molecular dynamics simulation. These three techniques were used in parallel to confirm a consistent trend between the three ILs. It was found that the IL with the smaller sized cation had a larger diffusion coefficient, leading to a higher capacitance at faster charge–discharge rates. Furthermore, the IL electrolyte performance was correlated with increasing temperature, which limited the voltage stability window and led to the formation of a solid electrolyte interphase on the carbon electrode surface, evident in both the CV and EIS experiments.

Keywords: ionic liquids, onion-like carbons, electrochemical capacitor, solid electrolyte interphase, diffusion coefficient

(Some figures may appear in colour only in the online journal)

1. Introduction

Electrochemical capacitors (ECs) are energy storage devices that bridge the gap between batteries and conventional dielectric and electrolytic capacitors. ECs are typically used for high power applications requiring a long cycle life, given that their lifetime can exceed 1 million charge–discharge cycles. Within ECs, there are electric double-layer capacitors (EDLCs) which store charge purely electrostatically, theoretically void of any chemical reactions. These EDLC devices are typically composed of a high surface area carbon electrode, an electrically insulating and ionically conducting separator, current collectors and an electrolyte [1, 2]. Upon charging of the carbon electrode, counter ions in the electrolyte reorient and move toward the electrode surface to balance the charge, creating an electric double layer (EDL) [3].

The carbon material of choice in a commercial EDLC is activated carbon, which has a surface area of ~1500 m^2 g^{-1} and an average pore size of ~1 nm [4]. Other carbon materials can also be used, such as graphene [5], carbon nanotubes (CNTs) [6], carbide-derived carbon (CDC) [7, 8] and onion-like carbon (OLC) [9–12], and these can be categorized as either endohedral or exohedral based on where the electrolyte ions reside with respect to their physical structure. Endohedral carbons (activated carbon and CDC) have porous networks within individual particles while exohedral carbons (CNTs, graphene and OLC) have little or no internal porosity, and most of their surface area accessible to electrolyte ions is on the outside of particles. This structural difference has consequences for EDLCs, in that ions in the EDL of an endohedral carbon experience additional ionic resistance, leading to decreased performance at faster charge–discharge rates [13]. Exohedral structures, while having a lower specific surface area, allow the use of more viscous electrolytes, such as neat ionic liquids (ILs), at room temperature.

In the case of exohedral carbon particles with a fixed surface area, the electrolyte properties dictate the performance of the resulting EDLC device. A low viscosity and high diffusion coefficient lead to a decreased ionic resistance and an enhanced power density as ions are able to efficiently move through the EDL at faster charge–discharge rates. The electrochemical stability window of the solvent dictates the energy density by equation (1):

$$E = \frac{1}{2} \times CV^2, \tag{1}$$

where C and V are the capacitance (F g^{-1}) and operating voltage (V) of the device [3].

Electrolytes for EDLCs can be classified into three categories based on their solvents. Aqueous electrolytes with water as the solvent, such as H_2SO_4 or KOH, have a maximum operating voltage of ~1.2 V, above which water splitting will occur. Organic electrolytes, typically with acetonitrile or propylene carbonate as the solvent, combined with a salt such as tetraethylammonium tetrafluoroborate (NEt_4-BF_4), have a maximum operating voltage of ~2.7 V. The third type of electrolyte that has proved promising for EDLCs is solvent-free ILs, which have a theoretical operating voltage up to 6 V depending on the cation–anion combinations [14]. In practice, the ion breakdown occurs at lower voltages due to interactions with the carbon electrode or the presence of moisture and other contaminants, but the practical voltage window (3–3.5 V) is still much higher than in aqueous and most organic electrolytes [15].

ILs can be considered as molten salts, like sodium chloride, which are liquid at ambient conditions, making them ideal for EDLCs. ILs are interesting for study in ECs because of their unique properties such as negligible vapor pressure, low melting point, high boiling point and chemical stability [16]. Although many ILs have been discovered, the ILs that are most extensively studied are those based on the dialkylimidazolium cation since when paired with the tetrafuoroborate anion, they are resistant to moisture traces [17]. These ions contain an alkyl chain that can vary in size and length. The capacitive effects of the alkyl chain length have been investigated experimentally as this structural difference affects properties such as viscosity and conductivity [18, 19]. Studies show that the capacitance of EDLCs decreases with increasing alkyl chain length of the cation in the IL [19, 20].

The diffusion coefficient (D) of electrolyte ions is an important parameter, as it can be used to relate physical properties such as ionic conductivity or viscosity, which have consequences for EDLC applications. However, when ions are confined in pores or on the surface of carbon, the diffusion rate can be strongly changed. While diffusion in porous carbons has been studied, specifically with aqueous electrolytes [21], diffusion of ILs at the surface of exohedral particles has not been investigated so far.

In this work, we show the results for ILs at the surface of OLC for EDLC applications. Diffusion coefficients were calculated from EIS and correlated with quasielastic neutron scattering (QENS) measurements and molecular dynamics (MD) simulations. OLC was used as the electrode material to reduce the added variable that nanopores would have on the system. In order to investigate the influence of the cation type, we use the same anion but three different cations in this study. The ILs used were 1-ethyl-3-methylimidazolium bis(trifluoromethylsulfonyl)imide [EMIM][Tf2N], 1-hexyl-3-methylimidazolium bis(trifluoromethylsulfonyl) imide [HMIM][Tf2N] and 1,6-bis(3-methylimidazolium-1-yl) bis(trifluoromethylsulfonyl)imide [BMIH][Tf2N]. Both [EMIM] and [HMIM] ions are monovalent (+1 charge), while [BMIH] is divalent (+2 charge).

2. Materials and experiment

OLC was made by annealing a nanodiamond precursor (UD90 grade, SP3 Diamond Technologies, USA) [22] at 1800 °C and applying a vacuum of ~10^{-6} Torr for 3 h in a custom-made vacuum furnace (Solar Atmospheres, USA). OLC has a ~5–7 nm diameter and a highly graphitic structure resembling that of an onion. Data previously published on this material [9] reports a surface area of ~450 m^2 g^{-1} and a broad pore size distribution from 3–20 nm, with 'pores' formed by voids between carbon particles.

Synthesis of [EMIM][Tf2N] [23], [HMIM][Tf2N] [24] and [BMIH][Tf2N] [25] was carried out according to established literature procedures. The notation for [EMIM] is created from E for ethyl, M for methyl and IM for imidazolium. [HMIM] is similar though the H is for hexyl. [BMIH] is unique in that B is for bis, M is for methyl, I is for imidazolium and H is for hexyl. The shape of this ion contains two methylimidazolium molecules connected by a hexyl.

OLC electrodes were made with the aid of 5 wt% polytetrafluoroethylene (PTFE) binder (60 wt% solution in water, Aldrich, USA). The OLC/PTFE composite was rolled to a thickness of 140 μm (weight of 7.0 mg) using a Durston rolling mill (UK) and electrodes were punched into 12 mm diameter discs. An electrically insulating and ionically conducting PTFE separator (Gore, USA) was used to prevent the short circuit of electrodes. Carbon-coated aluminum (Exopack, USA) was used to optimize the interface between the current collector and the carbon electrodes. The components, including the two identical electrodes, two carbon-coated discs and one piece of separator, were placed into a stainless steel Swagelok®

cell (USA) with ~1 ml of IL. The assembled cell was placed into a custom-made environmental chamber consisting of a Styrofoam box, an electric heating tape (HTS/Amptek, USA) and a temperature control box (iSeries, Omega, USA). Prior to the electrochemical measurements, the temperature was kept constant for a minimum of 1 h. Assembly and testing was performed in a dry argon-filled glove box.

Electrochemical measurements were performed using a VMP3 potentiostat (BioLogic, USA). Cyclic voltammetry (CV) was characterized by a two-electrode system symmetric cell in a 3 V electrochemical window for [EMIM][Tf2N] and [HMIM][Tf2N] and a 2 V electrochemical window for [BMIH][Tf2N]. The smaller voltage window is a result of initial studies, which found peaks at voltages above 2 V and 20 °C, indicating a redox process. For each IL, a single device was assembled and tested with the temperature increasing from 20 °C to 80 °C with 20 °C steps, and with a 1 h resting period at each temperature to allow the system to come to equilibrium before measuring the performance. The experiments were performed starting with EIS, followed by CV at different scan rates, and concluded with an additional EIS scan to evaluate any changes in the system that might have occurred during cycling at high voltages. EIS was performed at open circuit voltage (OCV) using a 10 mV amplitude at frequencies from 200 kHz to 10 mHz.

Referring specifically to EDLCs, EIS is a characterization technique that slightly perturbs the system by a sinusoidal voltage (typically ~10 mV s^{-1}) around its OCV and measures its current response within a range of frequencies, usually between 200 kHz and 10 mHz. At high frequencies, the system behaves as a resistor, with the current response being completely in phase with the voltage because ions are not able to move through the EDL at such high rates. The electronic resistance resulting from the carbon electrode or wires can be calculated from the *x*-intercept at high frequencies. At the lowest frequencies, the current should be –90° out of phase with the voltage, indicating that the ions have time to come to a steady state in the EDL and a purely capacitive system. In the mid-frequency range (~1–100 Hz), resistance associated with the ions in the electrolyte is seen as a ~45° line in a Nyquist plot. This transition point at which the slope of the Nyquist plot changes from 45° to 90° can be used to calculate the diffusion coefficient [26, 27], as shown in equation (2):

$$D = \omega R^2 \tag{2}$$

where D is the diffusion coefficient ($m^2\ s^{-1}$), ω is the 'knee frequency' at which the system transitions to a more capacitive behavior, and R is characteristic of the distance ions must travel (m), which differs between systems. In our investigations, R was the electrode thickness.

QENS is a special case of inelastic neutron scattering, which, in general, measures scattering intensity as a function of energy and momentum transfer from incident neutrons to the sample [28]. Unlike elastic scattering measured in neutron diffraction and small-angle neutron scattering experiments, or inelastic scattering originating from inter- or intra-molecular vibrations, quasielastic scattering is observed only when there are diffusion- or relaxation-type motions in the system studied. It manifests itself in the broadening of the elastic line with respect to the resolution profile. A diffusion process is observable if the associated QENS broadening (proportional to the diffusion coefficients) exceeds the width of the resolution function. The energy resolution of neutron backscattering spectrometers, which are dedicated to QENS measurements, is typically on the micro-eV scale, which allows measurements of diffusion dynamics on a time scale of up to a few nanoseconds. The shortest measurable time is limited by the accessible dynamic range of the spectrometer; too fast a dynamic process will yield a signal too broad to be measured. Typically, QENS experiments probe dynamics on a pico- to nano-second time scale. For many liquids, including ILs, the diffusion dynamics at near-ambient temperatures and in the moderately supercooled state falls in this range.

QENS experiments were done using the backscattering spectrometer at Oak Ridge National Laboratory, BASIS, which has a Q-averaged energy resolution of 3.5 μeV (full-width at half-maximum) [29]. The spectrometer was operated in the standard 60 Hz mode, and the dynamic range of ±100 μeV was chosen for the data analysis. The samples were placed in aluminum sample holders; their thickness was carefully controlled in order to minimize the effects of multiple neutron scattering in the samples.

The data were collected at the baseline temperature of 4 K and six different temperature points (260, 280, 300, 320, 340 and 360 K) above the melting temperature of the ILs. The data set collected at 4 K was used as the resolution function. The cation of ILs bears a number of hydrogen atoms whereas the anion has no hydrogen atoms. Since hydrogen is a very strong incoherent neutron scattering element, our QENS experiment predominantly probes the self-diffusion of the cations in these ILs. The dynamic structure factor, $S(Q, \omega)$, was deduced by normalizing the raw data to the vanadium standard, correcting for container scattering and interpolating to constant values of the momentum transfer, Q. Since the QENS signal originates mainly from the incoherent scattering by the hydrogen atoms, Fourier transformation of $S(Q, \omega)$ with subsequent normalization to unity at $t = 0$ yields the self-correlation function, $\Phi(Q, t)$.

The mean relaxation times of the α-process were obtained by fitting the $\Phi(Q, t)$ with the Kohlrausch–Williams–Watts (KWW) stretched exponential function [30] shown in equation (3):

$$\phi(Q,t) = f_q \exp\left[\frac{-t}{\tau_Q}\right]^{\beta}, \tag{3}$$

where τ_Q is the characteristic relaxation time and f_q is the Debye–Waller factor. The mean relaxation times were obtained by $\langle\tau\rangle = (\tau_Q/\beta)\Gamma(1/\beta)$, where Γ is the gamma function. The self-diffusion coefficients were obtained from the Q^2 dependence of relaxation times, which show a DQ^2 behavior in the Q range of 0.3–1.1 $Å^{-1}$ [31], by equation (4):

$$D = \lim_{Q\to 0} \frac{1}{\langle\tau\rangle Q^2} \tag{4}$$

where Q is the momentum transfer, $\langle\tau\rangle$ is the mean relaxation time and D is the diffusion coefficient.

MD simulation is one of the most powerful tools to investigate the complex structure, dynamic processes and

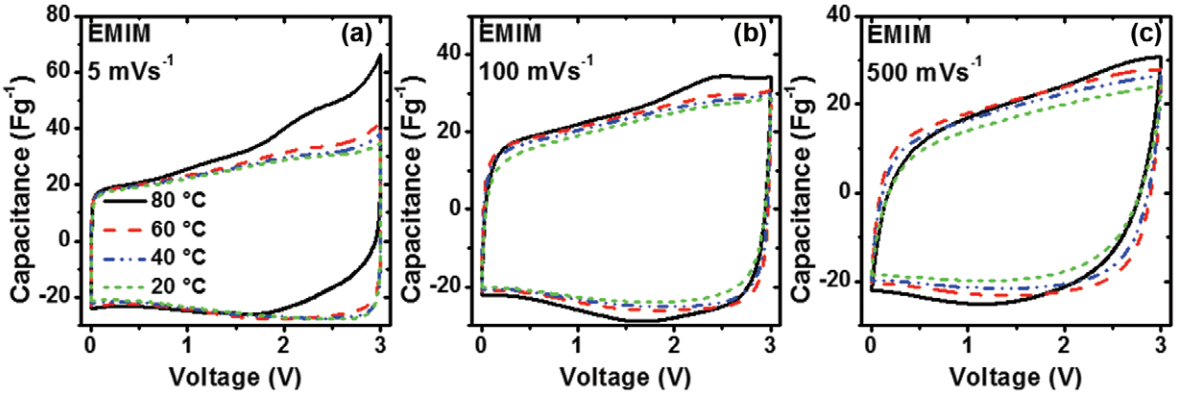

Figure 1. CVs of [EMIM][Tf2N] at (*a*) 5 mV s^{-1}, (*b*) 100 mV s^{-1} and (*c*) 500 mV s^{-1} for all four temperatures. Temperatures include 20, 40, 60 and 80 °C.

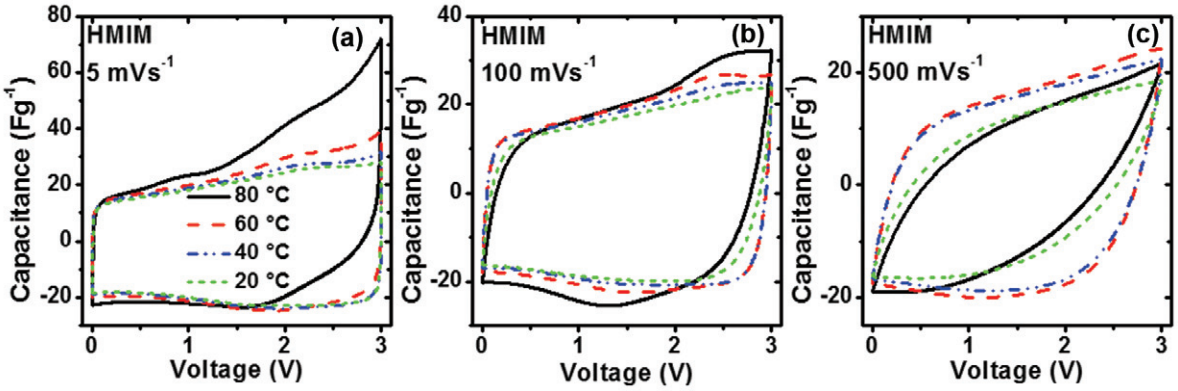

Figure 2. CVs of [HMIM][Tf2N] at (*a*) 5 mV s^{-1}, (*b*) 100 mV s^{-1} and (*c*) 500 mV s^{-1} for all four temperatures. Temperatures include 20, 40, 60 and 80 °C.

thermodynamic properties for many-body systems, and generates information at microscopic levels, including atomic positions and velocities. MD simulation is a suitable technique to explore the microscopic solid–liquid interfacial phenomena as well. It has been widely implemented in investigating the electrode–electrolyte interfaces, especially for carbon electrode–IL electrolyte interactions in EDLCs [32]. We have successfully predicted the electric double-layer structures of OLC/IL-based EDLCs in previous work [33–35]. The dynamic properties of IL electrolytes on carbon/silica surfaces have also been extensively studied, and the results from MD simulations exhibit good agreement with nuclear magnetic resonance measurements [36]. Thus, in this study, MD simulations were performed to characterize the interfacial dynamics of IL electrolytes on OLC electrode surfaces. The force field parameters for [BMIH] and [HMIM] were adapted from the all-atom force field developed by Yeganegi *et al* [37]. The force field of [Tf2N] was taken from the study of Canongia Lopes *et al* [38]. The deviation of the calculated density is within 5% compared to the experimental measurement [39]. All simulations in this work were performed using the MD package GROMACS [40]. The time step of 1 fs was used to integrate the equation of motion with the spherical cutoff of 1.1 nm in non-bonded van der Waals interactions. Long-range electrostatic interactions were treated by the particle mesh Ewald method [41]. All the C–H bonds were constrained during simulations and periodic boundary conditions were applied in three dimensions. OLC with a radius of 1.22 nm was completely frozen in the center of a box filled with IL throughout the simulations. The system was equilibrated using isothermal–isobaric ensemble at the target temperatures (300, 315, 330, 345 and 360 K) and 1 bar. After sufficient equilibration for 8 ns, 4 ns production runs were obtained to calculate the diffusion coefficient of cations. For the diffusion of ILs on OLC, the trajectory of ILs in the first layer close to the OLC surface at a thickness of 1.0 nm was used.

The diffusion coefficient was calculated according to the Einstein relation [42], as shown in equation (5):

$$D = \lim_{t\to\infty} \frac{1}{6t} \langle [r_i(t) - r_i(0)]^2 \rangle, \tag{5}$$

After linear fitting of the mean square displacement, the diffusion coefficient was obtained from the fitted slope divided by six. Note that in simulations, the diffusion coefficient of cations was calculated to represent the diffusion property of ILs and compared with experimental results.

3. Results

The electrochemical performance for [EMIM][Tf2N] in figure 1 shows cyclic voltammograms (CVs) normalized to their respective scan rates to present specific capacitance versus voltage. The results at 5 mV s^{-1} (figure 1(*a*)) show similar performance for 20, 40 and 60 °C, with their shapes being highly

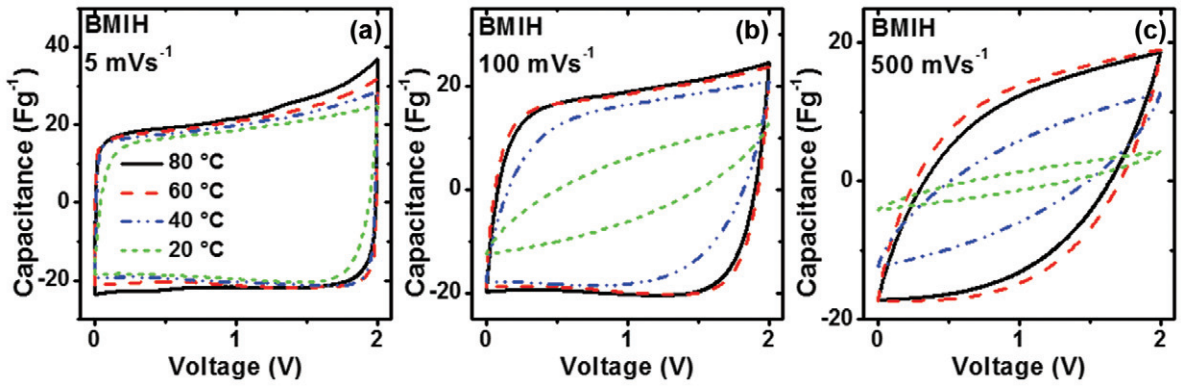

Figure 3. CVs of [BMIH][Tf2N] at (*a*) 5 mV s^{-1}, (*b*) 100 mV s^{-1} and (*c*) 500 mV s^{-1} for all four temperatures. Temperatures include 20, 40, 60 and 80 °C.

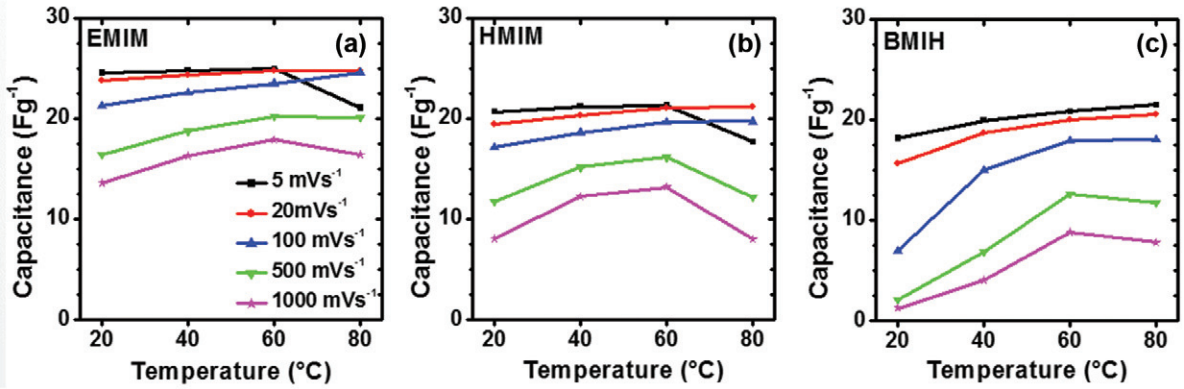

Figure 4. The capacitance as a function of temperature for (*a*) [EMIM][Tf2N], (*b*) [HMIM][Tf2N] and (*c*) [BMIH][Tf2N] taken from the CVs at a range of scan rates.

rectangular. At a higher temperature of 80 °C, an increase in capacitance (current) at higher voltages in the cathodic region indicates a decomposition of the IL. As a result of the reaction in the cathodic region, there is a delay in the current response in the anodic portion of the CV at 80 °C. At higher scan rates (figures 1(*b*) and (*c*)) and at 80 °C, the cathodic reaction at higher voltages is minimized because the voltage sweep is faster than the reaction kinetics. Because the reaction time constant is large, the kinetic-limited process cannot occur within the limited time at higher charge–discharge rates. The shape of the CV at the highest scan rate, 500 mV s^{-1} (figure 1(*c*)), remains highly rectangular at all temperatures for [EMIM][Tf2N].

The performance of [HMIM][Tf2N] at low scan rates (figure 2(*a*)) resembles [EMIM][Tf2N] (figure 1(*a*)). At temperatures of 20, 40 and 60 °C, [HMIM][Tf2N] has a highly capacitive, rectangular CV shape, while 80 °C shows a similar spike in the cathodic region and a delay in the anodic region due to chemical reactions above 2 V. At 100 mV s^{-1}, the cathodic current at high voltage scales with temperature. The CV curve at 80 °C is more resistive (lower slope) as the current changes polarization in the discharge curve. At the highest charge–discharge rate of 500 mV s^{-1} (figure 2(*c*)), [HMIM][Tf2N] has a more resistive CV curve at 20 °C compared to the CV curve of [EMIM][Tf2N] at 20 °C (figure 1(*c*)). The larger cation with the longer alkyl chain, [HMIM][Tf2N], experiences a larger ionic resistance which leads to a poorer performance at faster charge–discharge rates. Increasing the temperature to 40 and 60 °C reduces the ionic resistance, causing the shape of the CV at 500 mV s^{-1} (figure 2(*c*)) to be more capacitive than at room temperature.

Of the three cations we investigated, [BMIH] is the largest in size due to its dicationic structure. Additionally, it exhibits the most resistive CV curves out of the three ILs (figure 3). The results reported are for a potential window of 2 V since the electrolyte decomposition starts beyond this value at 20 °C [43]. [BMIH] is the only cation to consistently exhibit this decomposition between 2 and 3 V, especially at 80 °C. With the reduced potential window, the CV curves for all temperatures at 5 mV s^{-1} are highly capacitive (figure 3(*a*)). The effect of the large cation becomes evident when the scan rate is increased to 100 mV s^{-1} (figure 3(*b*)). At this rate, the CV curve at 20 °C is highly resistive, with almost no capacitance. This behavior is substantially worse than that for [EMIM][Tf2N] (figure 1(*b*)) and [HMIM][Tf2N] (figure 2(*b*)) under the same conditions. Elevating the temperature to 40, 60 and 80 °C reduces the ionic resistance, returning the curve to the desired rectangular shape and increasing the capacity. At the highest scan rate, 500 mV s^{-1}, the CV curve at 20 °C is almost completely resistive (figure 3(*c*)). Even at higher temperatures, the curves are highly resistive, indicating the cation's limit for a charge–discharge rate.

In figure 4, the capacitive performance as a function of temperature evaluated by CV is summarized at different scan

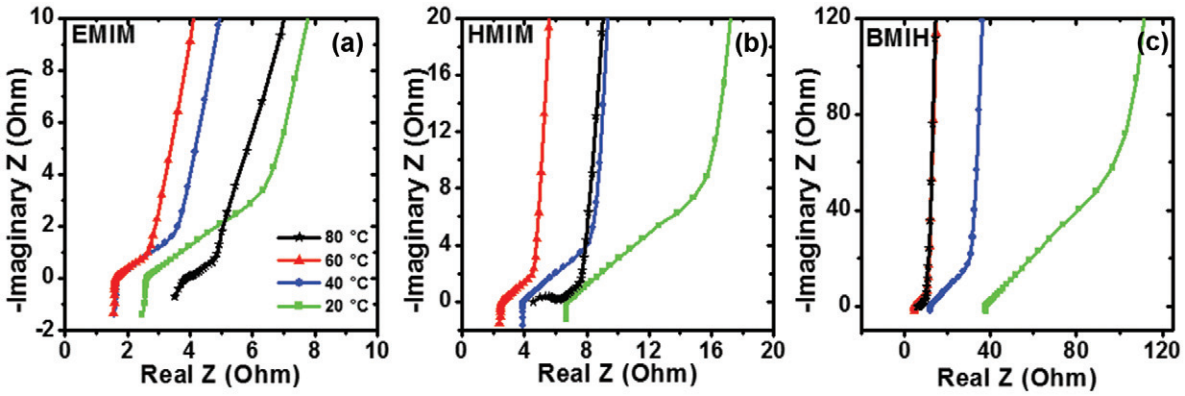

Figure 5. The Nyquist plots of impedance spectroscopy for (*a*) [EMIM][Tf2N], (*b*) [HMIM][Tf2N] and (*c*) [BMIH][Tf2N] for all four temperatures. The plots shown are zoomed in to better show the effect of temperature on the shape of the curves.

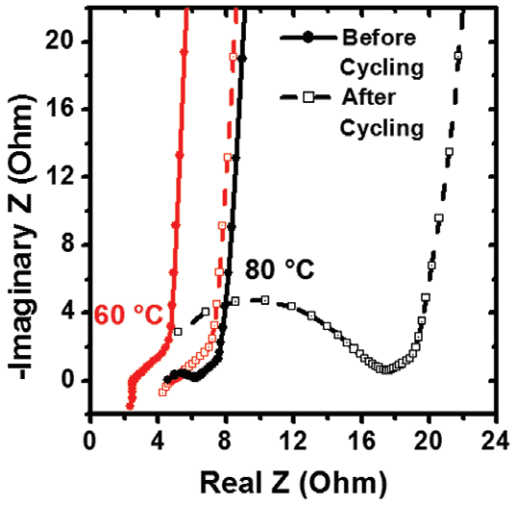

Figure 6. HMIM EIS data for 60 and 80 °C before and after the full set of cycling tests. A resistive SEI layer, indicated by a semicircle in the plot, develops significantly after cycling at 80 °C.

rates. Values for capacitance were calculated from the integral of the discharge curve in equation (6):

$$C = 2\frac{\int I\,\mathrm{d}V}{vVm}, \tag{6}$$

where C is the specific capacitance of one electrode normalized by mass (F g^{-1}), I is the current of the integrated discharge curve (A), v is the charge-discharge rate of the scan (V s^{-1}), V is the potential window for each cycle (V), m is the mass of one electrode (g) and the factor of 2 is used for the two capacitors in the series [44].

Comparison of figures 4(*a*)–(*c*) reveals a trend in capacitance among the three ILs. As the cation increases in size from EMIM to BMIH, the capacitance is generally lower for all corresponding temperatures and scan rates. This can be attributed to the higher ionic resistance that is characteristic of the larger, more viscous and less conductive cations [45–47]. It is also the reason for the resistive CV curves observed for [BMIH][Tf2N] in figure 3. Another interesting feature revealed in figures 4(*a*) and (*b*) is the sharp decline in capacitance at 5 mV s^{-1} and 80 °C. Since the capacitance is calculated from the integral of the CV discharge curve, this decrease can be attributed to the delay in current response discussed earlier for [EMIM][Tf2N] and [HMIM][Tf2N] (figures 1(*a*) and 2(*a*)). The change in the shape of the discharge curve reduces the area, thereby reducing the capacitance. In general, the behavior of the ILs at high scan rates is limited at 80 °C, shown by the last point on the curves in figure 4. It has been reported for similar ILs that as the temperature is increased, the size of the stable potential window decreases [43]. For example, the cathodic limit for [EMIM][Tf2N] is 1.55 V at 60 °C, and since the OCV potential of the cells is very close to zero, the cathodic potential for all experiments is about 1.5 V. Since this window decreases with increasing temperature, when the cell is tested at 80 °C, the stable window is even smaller and therefore less than the tested 1.5 V. Since the IL is not stable at this potential window, it will experience decomposition (discussed later) at voltages past the limit. In this case, we observe the capacitive effects of decomposition at 80 °C in the form of a drastic increase in the system's capacitance [43]. Due to the reduced potential window for the [BMIH][Tf2N] tests, this reaction does not occur, which is consistent with the curve at 5 mV s^{-1} in figure 4(*c*). Unlike [EMIM] and [HMIM], [BMIH] does not exhibit a sharp decrease in capacitance at 80 °C because for all temperatures, the cathodic potential was reduced to 1 V, which is less than the limit at all temperatures.

As stated before, with a net potential window of 3 V, the stability window of each electrode is variable, especially at higher temperatures [43]. Surpassing the stability window of an ion can lead to decomposition of that ion on its corresponding electrode. It has been shown that when [Tf2N] experiences a potential higher than its stability limit, reaction products form on the electrode surface, resulting in the formation of a solid electrolyte interphase (SEI) layer on the cathode [48]. While this predominantly occurs in lithium ion batteries, the behavior of the ion is similar, forming an SEI layer on the carbon electrode [48]. The exact reaction products are unknown for this system and although it is beyond the scope of this study, SEI formation in carbon supercapacitors warrants further investigation.

In addition to CV, impedance spectroscopy can also confirm these trends observed in the three ILs at varying temperatures (figure 5). Figures 5(*a*) and (*b*) show the Nyquist

plots for [EMIM][Tf2N] and [HMIM][Tf2N] at different temperatures. Since the ionic resistance is higher for ILs at room temperature, we can see that the value of the 'knee frequency' in the mid-frequency range is lowest at low temperatures (table 1). Features of the EIS plots, specifically the appearance of a semicircle at high frequencies [49] in figures 5(*a*) and (*b*), indicate the formation of an SEI layer, which is further evidence for the electrolyte decomposition revealed in figure 1(*a*). The comparison of EIS Nyquist plots before and after all the cycling tests for [HMIM][Tf2N] in a 3 V window yields further proof of SEI layer formation (figure 6). As temperature increases, the value of the knee frequency decreases and the *x*-intercept also moves closer to 0, which indicates a decrease in the electronic resistance of the system. However, the test at 80 °C appears to have the highest electronic resistance, which verifies the SEI formation that occurs at high temperatures. Since the tests were performed in order of increasing temperature, this indicates that cycling at 60 °C began the process of decomposition, affecting the following EIS test and the entire group of 80 °C tests. The high temperatures cause the anion [Tf2N] to deposit reaction products, forming an SEI layer on the carbon electrode. This additional electronically insulating layer on the cathode increases the electronic resistance of the system [50], corresponding to the *x*-intercept of the EIS curve. In addition to the total electronic resistance, an interfacial resistance is added between the components of the device due to the deposited film on the carbon electrode. This is represented by the appearance of a semicircle that accompanies the change in *x*-intercept of the Nyquist plots. The noticeable changes in the EIS plots at higher temperatures all suggest the formation of an SEI layer due to the anion reaction at potentials greater than the high temperature stability window. Finally, for [BMIH][Tf2N] (figure 5(*c*)), the Nyquist plot for 80 °C does not indicate similar changes in the electrolyte chemistry because the reduced voltage window removed any possible decomposition of the electrolyte. As a result, the electronic and interfacial resistance is not negatively affected at this high temperature as with [EMIM][Tf2N] and [HMIM][Tf2N].

Diffusion coefficients (*D*) for the three ILs were calculated by three different experimental techniques and are shown in Arrhenius plots (figure 7). EIS data were analyzed according to equation (2). From this relationship, which effectively normalizes the knee frequency by the electrode thickness, *D* is characteristic of the motion of ions throughout the bulk electrode (figure 7(*a*)). For all three techniques, the trend is followed with the diffusion coefficient decreasing with increasing cation size, with [EMIM][Tf2N] maintaining the fastest *D* and [BMIH][Tf2N] having the slowest. Additionally, for all three ILs, the diffusion coefficient increases with increasing temperature. By increasing the temperature of the system, the resistance of the IL electrolyte is decreased [6], which in turn increases the value of the knee frequency in impedance spectroscopy (figure 6). Since the thickness of the electrodes remains constant, the increasing knee frequency causes the increase in *D*, consistent with the values shown in table 1.

Table 1. Values for the 'knee frequency' (Hz) at each temperature for each IL.

	Frequency (Hz)		
Temperature (°C)	[EMIM]	[HMIM]	[BMIH]
20	1.612	0.499	0.071
40	2.382	1.089	0.228
60	5.208	2.382	0.738
80	7.705	3.519	1.612

The relatively small slope of the lines in figure 7(*a*) indicates that temperature has a less significant effect on the diffusion coefficient. Since the system includes an applied potential and therefore a charged OLC surface, the velocity of the ions through the film electrode is increased, evident in the higher diffusion coefficients in the range of 10^{-9}–10^{-6} m^2 s^{-1}. For QENS, the diffusion coefficient of the bulk IL without a charged electrode surface was measured. The inability of the charged surface to initiate movement of the ions leads to values that are smaller by three orders of magnitude (figure 7(*b*)) compared to the EIS results. The smaller *D* values on the order of 10^{-11}–10^{-10} m^2 s^{-1} are consistent with those reported from previous studies involving uncharged systems and calculated self-diffusion coefficients [51]. However, the diffusion coefficients calculated from MD simulations are on the order of 10^{-12}–10^{-11} m^2 s^{-1} (figure 7(*c*)). This can be explained by the difference between the bulk and interfacial behavior of the ILs. The bulk ILs measured in QENS behave differently to ILs at an OLC surface calculated from MD simulations. It is known that the ions located in the adsorbed layer of carbon surfaces exhibit slower dynamics than bulk ILs due to the denser ion packing at the interface caused by the attractive interaction energy between ILs and carbon surfaces.

Transitioning to QENS (figure 7(*b*)), this technique was used to analyze the behavior of pure ILs without OLC. Fourier transformation of $S(Q, \omega)$ obtained from the raw data yields the self-correlation function, $\Phi(Q, t)$, shown in figure 8. This function was fit using equation (3) to calculate the mean relaxation time. Using these values and equation (4), diffusion coefficients were calculated and can be compared to the other techniques (figure 7). The diffusion coefficient calculated is that of the bulk IL without a charged surface to initiate movement of the ions. This can explain why the values for *D* are smaller by three orders of magnitude, since the neutrally charged system does not increase the speed of the ions. These smaller values on the order of 10^{-11} are consistent with those reported from previous studies involving uncharged systems and calculated self-diffusion coefficients [51].

In contrast to the diffusion measured in EIS, the slower diffusion coefficients from MD are smaller by a few orders of magnitude, which can also be attributed to the uncharged nature of the system and the simplified electrode model used in the simulation. In addition, the diffusion coefficients obtained from the QENS and MD simulation are significantly lower in contrast with those from the EIS tests, indicating the effect of adding an electric field to the system. Although the techniques differ slightly in the type of diffusion they are measuring, the trends are clear for all temperatures, showing that *D* for EMIM > HMIM > BMIH.

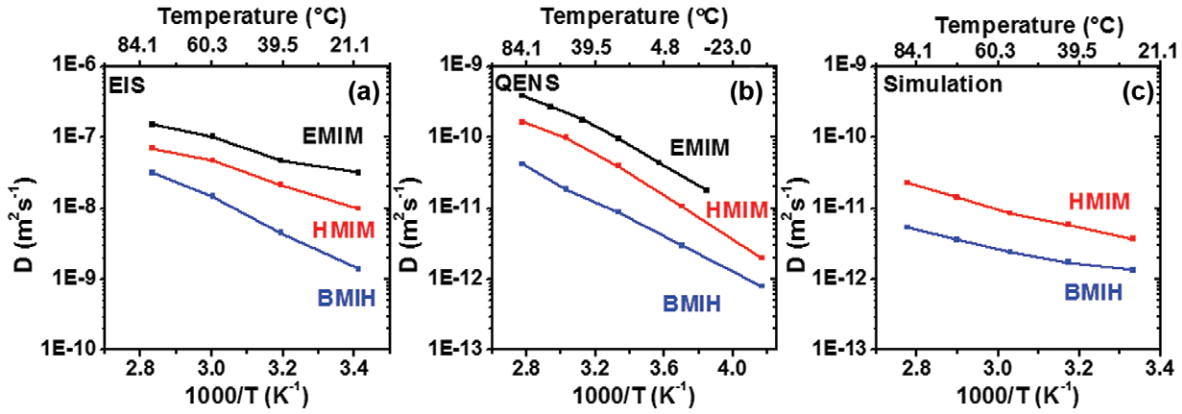

Figure 7. The diffusion coefficients for all three ILs calculated using (*a*) electrochemical impedance spectroscopy of ILs on OLC electrodes, (*b*) QENS for bulk ILs and (*c*) MD simulation for ILs at the surface of OLC. The diffusion coefficient is plotted as a function of temperature.

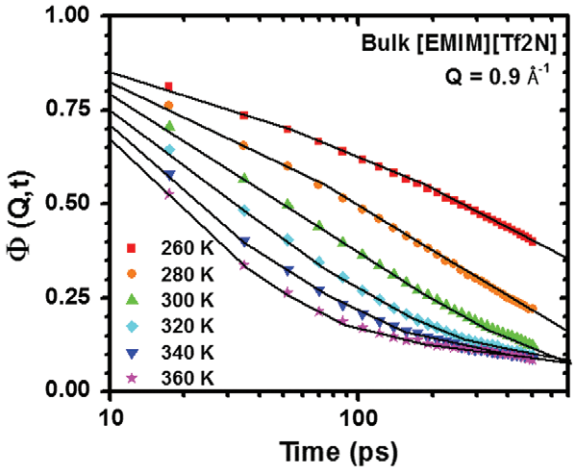

Figure 8. The self-correlation function of EMIM cations in EMIM-Tf2N IL at a Q value of 0.9 Å^{-1}. The solid lines are fit with KWW function with a β value of 0.5.

This study validates the use of EIS for measuring the diffusion coefficient of IL electrolytes under an electric field. Depending on the instruments, techniques and experimental conditions (bulk or interface), different values of diffusion coefficients may be obtained as shown by the three plots in figure 7. However, the consistency of the trends from EIS, QENS and MD observed in this study is expected for other ILs, including possible multivalent ones.

4. Conclusion

The electrochemical performance and stability of three ILs with varying cations and an identical anion ([EMIM][Tf2N], [HMIM][Tf2N] and [BMIH][Tf2N]) were investigated as a function of temperature, using OLC as the electrode material. It was found that the capacitance decreases and the ionic resistance increases as cation size increases, meaning EMIM had the highest capacitance and lowest ionic resistance, while BMIH had the lowest capacitance and the highest ionic resistance. All three ILs showed better performance as the temperature was increased up to 60 °C. Decomposition of the [Tf2N] anion due to voltage stability window limitations at temperatures at or above 80 °C resulted in the formation of an SEI layer on the carbon surface. This causes a decrease in capacitance and an increase in interfacial and electronic resistance for the system, which is confirmed by multiple electrochemical techniques. Diffusion coefficients obtained from EIS, QENS and MD simulations as a function of temperature support the electrochemical measurements showing the IL with the smaller cation having faster diffusion than the larger cation. The difference in charge between BMIH and the other two cations did not seem to have an effect on performance.

Acknowledgments

This work was supported as part of the Fluid Interface Reactions, Structures, and Transport (FIRST) Center, an Energy Frontiers Research Center funded by the Office of Science, Office of Basic Energy Sciences, US Department of Energy. Part of this research conducted at Oak Ridge National Laboratory's Spallation Neutron Source was sponsored by the Scientific User Facilities Division, Office of Basic Energy Sciences, US Department of Energy. SL acknowledges the National Energy Research Scientific Computing Center (NERSC) for providing the computation time, which is supported by the Office of Science of the US Department of Energy under Contract No DE-AC02-05CH11231.

References

[1] Simon P and Gogotsi Y 2010 Charge storage mechanism in nanoporous carbons and its consequence for electrical double layer capacitors *Phil. Trans. R. Soc.* A **368** 3457–67
[2] Béguin F and Frackowiak E 2010 *Carbons for Electrochemical Energy Storage and Conversion Systems* (Boca Raton, FL: CRC Press)
[3] Conway B E 1999 *Electrochemical Supercapacitors: Scientific Fundamentals and Technological Applications* (New York: Plenum)
[4] Barbieri O, Hahn M, Herzog A and Kötz R 2005 Capacitance limits of high surface area activated carbons for double layer capacitors *Carbon* **43** 1303–10

[5] Stoller M D, Park S, Zhu Y, An J and Ruoff R S 2008 Graphene-based ultracapacitors *Nano Lett*. **8** 3498–502

[6] Lin R *et al* 2011 Capacitive energy storage from −50 to 100 °C using an ionic liquid electrolyte *J. Phys. Chem. Lett*. **2** 2396–401

[7] Pérez C R *et al* 2013 Structure and electrochemical performance of carbide-derived carbon nanopowders *Adv. Funct. Mater*. **23** 1081–9

[8] Chmiola J *et al* 2005 Double-layer capacitance of carbide derived carbons in sulfuric acid *Electrochem. Solid-State. Lett*. **8** A357–60

[9] McDonough J K *et al* 2012 Influence of the structure of carbon onions on their electrochemical performance in supercapacitor electrodes *Carbon* **50** 3298–309

[10] McDonough J K and Gogotsi Y 2013 Carbon onions: synthesis and electrochemical applications *Electrochem. Soc. Interface* **22** 61–6

[11] Plonska-Brzezinska M E and Echegoyen L 2013 Carbon nano-onions for supercapacitor electrodes: recent developments and applications *J. Mater. Chem.* A **2013** 13703–14

[12] Bushueva E G *et al* 2008 Double layer supercapacitor properties of onion-like carbon materials *Phys. Status Solidi b* **245** 2296–9

[13] Huang J S, Sumpter B G, Meunier V, Yushin G, Portet C and Gogotsi Y 2010 Curvature effects in carbon nanomaterials: exohedral versus endohedral supercapacitors *J. Mater. Res*. **25** 1525–31

[14] Lazzari M, Mastragostino M and Soavi F 2007 Capacitance response of carbons in solvent-free ionic liquid electrolytes *Electrochem. Commun*. **9** 1567–72

[15] Simon P and Gogotsi Y 2012 Capacitive energy storage in nanostructured carbon–electrolyte systems *Acc. Chem. Res*. **46** 1094–103

[16] Welton T 1999 Room-temperature ionic liquids. Solvents for synthesis and catalysis *Chem. Rev*. **99** 2071–84

[17] Galiński M, Lewandowski A and Stępniak I 2006 Ionic liquids as electrolytes *Electrochim. Acta* **51** 5567–80

[18] Su Y, Yan J, Li M, Zhang M and Mao B 2012 Electric double layer of Au(1 0 0)/imidazolium-based ionic liquids interface: effect of cation size *J. Phys. Chem. C* **117** 205–12

[19] Lockett V, Sedev R, Ralston J, Horne M and Rodopoulos T 2008 Differential capacitance of the electrical double layer in imidazolium-based ionic liquids: influence of potential, cation size, and temperature *J. Phys. Chem. C* **112** 7486–95

[20] Lockett V, Horne M, Sedev R, Rodopoulos T and Ralston J 2010 Differential capacitance of the double layer at the electrode/ionic liquids interface *Phys. Chem. Chem. Phys*. **12** 12499–512

[21] Suzuki M and Fujii T 1982 Concentration dependence of surface diffusion coefficient of propionic acid in activated carbon particles *AIChE* J. **28** 380–5

[22] Kuznetsov V L, Chuvilin A L, Butenko Y V, Malkov I Y and Titov VM 1994 Onion-like carbon from ultra-disperse diamond *Chem. Phys. Lett*. **222** 343–8

[23] Bulut S *et al* 2011 Temperature dependence of the viscosity and conductivity of mildly functionalized and non-functionalized $[Tf_2N]^-$ ionic liquids *Chem. Phys. Chem.* **12** 2296–310

[24] Fujii K *et al* 2011 Experimental evidences for molecular origin of low-Q peak in neutron/x-ray scattering of 1-alkyl-3-methylimidazolium bis(trifluoromethanesulfonyl) amide ionic liquids *J. Chem. Phys*. **135** 244502

[25] Cho W-J, Yeom C G, Kim B C, Kim K M, Ko J M and Yu K-H 2013 Supercapacitive properties of activated carbon electrode in organic electrolytes containing single- and double-cationic liquid salts *Electrochim. Acta* **89** 807–13

[26] Paasch G, Micka K and Gersdorf P 1993 Theory of the electrochemical impedance of macrohomogeneous porous electrodes *Electrochim. Acta* **38** 2653–62

[27] Yu P, Popov B N, Ritter J A and White R E 1999 Determination of the lithium ion diffusion coefficient in graphite *J. Electrochem. Soc*. **146** 8–14

[28] Bée M and Bee M 1988 *Quasielastic Neutron Scattering: Principles and Applications in Solid State Chemistry, Biology and Materials Science* (Bristol: Adam Hilger)

[29] Mamontov E and Herwig K W 2011 A time-of-flight backscattering spectrometer at the Spallation Neutron Source, BASIS *Rev. Sci. Instrum*. **82** 085109

[30] Kohlrausch R 1854 Theory of the electrical residue in the Leiden bottle *Pogg. Ann. Phys. Chem*. **91** 179–214

[31] Boon J and Yip S 1980 *Molecular Hydrodynamics* (New York: McGraw-Hill)

[32] Feng G, Li S, Presser V and Cummings P T 2013 Molecular insights into carbon supercapacitors based on room-temperature ionic liquids *J. Phys. Chem. Lett*. **4** 3367–76

[33] Feng G, Jiang D-E and Cummings P T 2012 Curvature effect on the capacitance of electric double layers at ionic liquid/onion-like carbon interfaces *J. Chem. Theory Comput*. **8** 1058–63

[34] Li S *et al* 2012 Molecular dynamics simulation study of the capacitive performance of a binary mixture of ionic liquids near an onion-like carbon electrode *J. Phys. Chem. Lett*. **3** 2465–9

[35] Li S, Van Aken K L, McDonough J K, Feng G, Gogotsi Y and Cummings P T 2014 The electrical double layer structure of dicationic ionic liquids at onion-like carbon surface *J. Phys. Chem.* C at press doi:10.1021/jp409888f

[36] Li S, Han K S, Feng G, Hagaman E W, Vlcek L and Cummings P T 2013 Dynamic and structural properties of room-temperature ionic liquids near silica and carbon surfaces *Langmuir* **29** 9744–9

[37] Yeganegi S, Soltanabadi A and Farmanzadeh D 2012 Molecular dynamic simulation of dicationic ionic liquids: effects of anions and alkyl chain length on liquid structure and diffusion *J. Phys. Chem.* B **116** 11517–26

[38] Canongia Lopes J N, Deschamps J and Pádua A A H 2004 Modeling ionic liquids using a systematic all-atom force field *J. Phys. Chem.* B **108** 2038–47

[39] Shirota H, Mandai T, Fukazawa H and Kato T 2011 Comparison between dicationic and monocationic ionic liquids: liquid density, thermal properties, surface tension, and shear viscosity *J. Chem. Eng. Data* **56** 2453–9

[40] Berendsen H J C, van der Spoel D and van Drunen R 1995 GROMACS: a message-passing parallel molecular dynamics implementation *Comput. Phys. Commun*. **91** 43–56

[41] Essmann U, Perera L, Berkowitz M L, Darden T, Lee H and Pedersen L G 1995 A smooth particle mesh Ewald method *J. Chem. Phys*. **103** 8577–93

[42] McQuarrie D 1976 *Statistical Mechanics* (New York: Harper and Row)

[43] Costa R, Pereira C M and Silva F 2010 Double layer in room temperature ionic liquids: influence of temperature and ionic size on the differential capacitance and electrocapillary curves *Phys. Chem. Chem. Phys*. **12** 11125–32

[44] Pech D *et al* 2010 Ultrahigh-power micrometre-sized supercapacitors based on onion-like carbon *Nature Nanotechnol*. **5** 651–4

[45] Bonhôte P, Dias A-P, Papageorgiou N, Kalyanasundaram K and Grätzel M 1996 Hydrophobic, highly conductive ambient-temperature molten salts *Inorg. Chem*. **35** 1168–78

[46] Widegren J A and Magee J W 2007 Density, viscosity, speed of sound, and electrolytic conductivity for the ionic liquid 1-hexyl-3-methylimidazolium bis(trifluoromethylsulfonyl) imide and its mixtures with water *J. Chem. Eng. Data* **52** 2331–8

[47] Anderson J L, Ding R, Ellern A and Armstrong D W 2004 Structure and properties of high stability geminal dicationic ionic liquids *J. Am. Chem. Soc*. **127** 593–604

[48] Howlett P C, Brack N, Hollenkamp A F, Forsyth M and MacFarlane D R 2006 Characterization of the lithium surface in *N*-methyl-*N*-alkylpyrrolidinium bis(trifluoromethanesulfonyl)amide room-temperature ionic liquid electrolytes *J. Electrochem. Soc*. **153** A595–606

[49] Xiao J *et al* 2011 Investigation of the rechargeability of Li–O_2 batteries in non-aqueous electrolyte *J. Power Sources* **196** 5674–8

[50] Frackowiak E and Beguin F 2002 Electrochemical storage of energy in carbon nanotubes and nanostructured carbons *Carbon* **40** 1775–87

[51] Weingärtner H 2008 Understanding ionic liquids at the molecular level: facts, problems, and controversies *Angew. Chem. Int. Edn.* **47** 654–70